Theoretical solution to second-harmonic generation of ultrashort laser pulse

Chen-Yang Hu, Hui-Jun He, Bao-Qin Chen, Zhi-Yi Wei, and Zhi-Yuan Li

Citation: Journal of Applied Physics **122**, 243105 (2017); doi: 10.1063/1.4998499
View online: https://doi.org/10.1063/1.4998499
View Table of Contents: http://aip.scitation.org/toc/jap/122/24
Published by the American Institute of Physics

Theoretical solution to second-harmonic generation of ultrashort laser pulse

Chen-Yang Hu,[1,2] Hui-Jun He,[1,2] Bao-Qin Chen,[3] Zhi-Yi Wei,[1] and Zhi-Yuan Li[3,a)]
[1]*Laboratory of Optical Physics, Institute of Physics, Chinese Academy of Sciences, P.O. Box 603, Beijing 100190, China*
[2]*University of Chinese Academy of Sciences, Beijing 100049, China*
[3]*College of Physics and Optoelectronics, South China University of Technology, Guangzhou 510640, China*

(Received 1 August 2017; accepted 9 December 2017; published online 29 December 2017)

We propose a theoretical method called the broadband nonlinear coupled wave theory (BNCWT) to evaluate the second harmonic generation (SHG) process of ultrashort laser pulse transporting in nonlinear media. Because of the broadband nature of the pulse laser, all the relevant second-order nonlinear interactions for different frequency components are considered in the analysis and simulation, including sum-frequency generation (SFG) and SHG. The SHG of an ultrashort pulse can be regarded as a series of self-SFG and self-SHG processes for different frequency components, and their mutual coupling. The solution of the problem traces back to the solution of a set of nonlinear coupled wave equations satisfied by all frequency components involved within the laser pulse. Numerical simulations show great consistency with experimental results, indicating that the proposed BNCWT is instructive and efficient and can have great practical value for experimental prediction. *Published by AIP Publishing*. https://doi.org/10.1063/1.4998499

I. INTRODUCTION

Optical second harmonic generation (SHG) and other nonlinear optical processes such as sum-frequency generation (SFG) and difference-frequency generation (DFG) contribute several of the most important mechanisms in obtaining efficient nonlinear frequency conversion of lasers and have been widely employed to serve practical needs in optics and laser sciences. In these processes, the birefringent phase matching (BPM) scheme and quasi-phase-matching (QPM) scheme have been used to maintain the match of relative phase,[1] so that efficient energy transfer among the interacting waves could occur. In recent years, along with the rapid development of ultrafast laser technologies, many innovative works have been done, such as the synthesis and time-resolved measurement of ultrashort pulse[2–5] and the generation of supercontinuum laser.[6,7] In order to gain full understanding of the underlying physics and to reach higher energy conversion efficiency, a theoretical approach enabling thorough analysis of nonlinear interaction of ultrashort pulse is highly desirable.

In the early 1960s, Armstrong *et al*. published the earliest theoretical work.[1] The interaction between light and nonlinear material can be routinely described by nonlinear coupled wave equations. Efficient energy transfer is expected to occur when the phase matching condition is satisfied. Several numerical methods have been established and applied to simulate second-order nonlinear interactions, including the split-step method,[8,9] Fourier-space method,[10–13] and effective nonlinear susceptibility model.[14–18] However, when the incident light is the ultrashort laser pulse, the involved electrical fields cannot be described as a monochromatic field; thus, the previous numerical methods no longer hold.[9,15,16]

In this work, we present an innovative theoretical method called the broadband nonlinear coupled wave theory (BNCWT) to simulate second-order nonlinear interactions of ultrashort pulse laser in nonlinear media. As an ultrashort laser pulse always involves a broadband spectrum of frequency component, in order to give a comprehensive description of the nonlinear interactions, all relevant contributing nonlinear processes for these frequency components need to be considered in the numerical simulation. This renders the solution of a series of nonlinear coupled wave equations. The spectral evolution and the conversion efficiency can be obtained. As a demonstrating example, the method has been applied to evaluate the SHG process in a 1 mm-thick β-barium borate (β-BBO) pumped by a 1 mJ 40 fs Ti:sapphire regenerative amplifier. Favorable consistency between the numerical simulations and experimental results is found. The basic principle of the numerical method gives a more comprehensive understanding that even the simplest nonlinear interaction as SHG of pulse laser should be regarded as a combined effect of a chain of many second-order nonlinear interacting processes including SHG and SFG taking place simultaneously within the nonlinear medium. The proposed BNCWT can be of great practical value for precise experimental prediction and optimization.

II. THEORETICAL MODEL AND FORMALISMS

The wave equations that describe optical wave propagation and interaction in a general medium is

$$\nabla^2\mathbf{E}(\mathbf{r},t) = \mu_0\varepsilon_0\frac{\partial^2\mathbf{E}(\mathbf{r},t)}{\partial t^2} + \mu_0\frac{\partial^2\mathbf{P}(\mathbf{r},t)}{\partial t^2}, \tag{1}$$

which is derived from Maxwell's equations. When the incident wave is an ultrashort laser pulse, the incident electric field $\mathbf{E}(\mathbf{r}, t)$ can be decomposed by Fourier transform

a)phzyli@scut.edu.cn

$$\mathbf{E}(\mathbf{r},t)=\int_{-\infty}^{+\infty}\mathbf{E}(\omega,\mathbf{r})e^{-i\omega t}d\omega, \tag{2}$$

which involves multiple frequency components. The electric polarization $\mathbf{P}(\mathbf{r}, t)$ involves both the linear polarization and nonlinear polarization and can be written as

$$\mathbf{P}(\mathbf{r},t)=\mathbf{P}^{(1)}(\mathbf{r},t)+\mathbf{P}_{NL}^{(2)}(\mathbf{r},t)+\cdots, \tag{3}$$

$$\mathbf{P}^{(1)}(\mathbf{r},t)=\varepsilon_0\int_{-\infty}^{+\infty}\chi^{(1)}(\omega)\mathbf{E}(\omega,\mathbf{r})e^{-i\omega t}d\omega, \tag{4}$$

$$\mathbf{P}_{NL}^{(2)}(\mathbf{r},t)=\varepsilon_0\int_{-\infty}^{+\infty}d\omega_1\int_{-\infty}^{+\infty}d\omega_2\boldsymbol{\chi}^{(2)}(\omega_1,\omega_2):\mathbf{E}(\omega_1,\mathbf{r})\mathbf{E}(\omega_2,\mathbf{r})e^{-i(\omega_1+\omega_2)t}, \tag{5}$$

where $\mathbf{E}(\omega, \mathbf{r})$, the position dependent electric field, represents the amplitude of the monochromatic wave at the angular frequency ω. Overall the function $\mathbf{E}(\omega, \mathbf{r})$ describes the frequency spectrum of the pulse laser. $\boldsymbol{\chi}^{(2)}(\omega_1, \omega_2)$ is the second-order nonlinear susceptibility tensor. Higher-order terms are neglected in our analysis here.

As shown in Eq. (2), an ultrashort laser pulse involves a series of frequency components. When the duration of the ultrashort pulse is down to tens of femtosecond, the corresponding frequency spectrum has tens of nanometer bandwidth. It can no longer be described by a monochromatic electric field. When such a laser pulse with high intensity transports in a nonlinear medium, even for a simple SHG process, multiple nonlinear processes other than SHG could take place simultaneously and all these nonlinear interactions must be taken into account in order to fully evaluate the physics of SHG. This of course will lead to much increasing complexity against conventional SHG for monochromatic optical waves. However, complexity is necessary for yielding a correct and accurate evaluation of the physical problem of pulse laser nonlinear optics.

In order to solve the above equations, we regard the pulse spectrum as a series of discrete frequency components, which look like a series of light comb with corresponding bandwidth $\Delta\omega$. Then, the continuous Fourier transform of Eq. (2) reduces to discrete Fourier series

$$\mathbf{E}(\mathbf{r},t)=\sum\mathbf{E}(\omega,\mathbf{r})e^{-i\omega t}\Delta\omega=\sum\mathbf{E}_{eff}(\omega,\mathbf{r})e^{-i\omega t}. \tag{6}$$

Here, $\mathbf{E}_{eff}(\omega,\mathbf{r}) = \mathbf{E}(\omega,\mathbf{r})\Delta\omega$, which can be regarded as the effective field amplitude for a monochromatic wave centered at ω. In this way, the corresponding pulse can be described by such a type of light comb. We also assume that Eqs. (4) and (5) follow the same discrete rule as $d\omega = d\omega_1 = d\omega_2 = \Delta\omega$. As a result, the linear polarization and nonlinear polarization can be unified as the following forms:

$$\begin{aligned}\mathbf{P}^{(1)}(\mathbf{r},t)&=\varepsilon_0\sum_{\omega}\chi^{(1)}(\omega)\mathbf{E}(\omega,\mathbf{r})e^{-i\omega t}\Delta\omega\\&=\varepsilon_0\sum_{\omega}\chi^{(1)}(\omega)\mathbf{E}_{eff}(\omega,\mathbf{r})e^{-i\omega t},\end{aligned} \tag{7}$$

$$\begin{aligned}\mathbf{P}_{NL}^{(2)}(\mathbf{r},t)&=\varepsilon_0\sum_{\omega_1}\sum_{\omega_2}\boldsymbol{\chi}^{(2)}(\omega_1,\omega_2)\\&\quad:\mathbf{E}(\omega_1,\mathbf{r})\Delta\omega\mathbf{E}(\omega_2,\mathbf{r})\Delta\omega e^{-i(\omega_1+\omega_2)t}\\&=\varepsilon_0\sum_{\omega_1}\sum_{\omega_2}\boldsymbol{\chi}^{(2)}(\omega_1,\omega_2)\\&\quad:\mathbf{E}_{eff}(\omega_1,\mathbf{r})\mathbf{E}_{eff}(\omega_2,\mathbf{r})e^{-i(\omega_1+\omega_2)t}.\end{aligned} \tag{8}$$

To see how we handle the pulse propagation, we first consider the situation without nonlinear polarization ($\mathrm{P}_{NL}^{(2)} = 0$). By substituting Eqs. (6) and (7) into Eq. (1), we find

$$\begin{aligned}\sum_{\omega}\nabla^2\mathbf{E}_{eff}(\omega,\mathbf{r})e^{-i\omega t}&=-\mu_0\varepsilon_0\sum_{\omega}\omega^2\mathbf{E}_{eff}(\omega,\mathbf{r})e^{-i\omega t}\\&\quad-\mu_0\varepsilon_0\sum_{\omega}\omega^2\chi^{(1)}(\omega)\mathbf{E}_{eff}(\omega,\mathbf{r})e^{-i\omega t}.\end{aligned} \tag{9}$$

Considering each frequency component, we have

$$\begin{aligned}\nabla^2\mathbf{E}_{eff}(\omega)&=-\omega^2\mathbf{E}_{eff}(\omega)-\mu_0\varepsilon_0\omega^2\chi^{(1)}(\omega)\mathbf{E}_{eff}(\omega)\\&=-\mu_0\varepsilon_0\omega^2\varepsilon(\omega)\mathbf{E}_{eff}(\omega),\end{aligned} \tag{10}$$

where $\varepsilon(\omega) = 1 + \chi^{(1)}(\omega)$ is the dielectric constant. Note that the solution for Eq. (10) follows the form

$$\mathbf{E}_{eff}(\omega,\mathbf{r})=\mathbf{a}(\omega)E_{eff}(\omega)e^{ik(\omega)z}.$$

Here, $\mathbf{a}(\omega)$ is the unit vector of electric field polarization and $E_{eff}(\omega)$ is the amplitude. Substituting the above term of solution into Eq. (10), we have

$$\begin{aligned}&\frac{\partial^2E_{eff}(\omega)}{\partial z^2}e^{ik(\omega)z}+2ik(\omega)\frac{\partial E_{eff}(\omega)}{\partial z}e^{ik(\omega)z}\\&\quad-k^2(\omega)E_{eff}(\omega)e^{ik(\omega)z}=-\mu_0\varepsilon_0\omega^2\varepsilon(\omega)E_{eff}(\omega)e^{ik(\omega)z}.\end{aligned} \tag{11}$$

Considering the slowly varying amplitude approximation, Eq. (11) becomes

$$2ik(\omega)\frac{\partial E_{eff}(\omega)}{\partial z}-k^2(\omega)E_{eff}(\omega)=-\mu_0\varepsilon_0\omega^2\varepsilon(\omega)E_{eff}(\omega). \tag{12}$$

If the medium has no loss, the corresponding electric field does not vary with distance z, namely, $\partial E_{eff}(\omega)/\partial z = 0$, so we have

$$-k^2(\omega)\mathbf{a}(\omega)+\mu_0\varepsilon_0\omega^2\varepsilon(\omega)\mathbf{a}(\omega)=0. \tag{13}$$

This is just the dispersion relation $\omega \sim k$ of each monochromatic wave.

In the next step, we consider the situation with the nonlinear polarization $\mathrm{P}_{NL}^{(2)}$. We substitute Eqs. (6), (7), and (8) into Eq. (1) and find

$$\begin{aligned}\sum_{\omega}\nabla^2\mathbf{E}_{eff}(\omega,\mathbf{r})e^{-i\omega t}&=-\mu_0\varepsilon_0\sum_{\omega}\varepsilon(\omega)\omega^2\mathbf{E}_{eff}(\omega,\mathbf{r})e^{-i\omega t}\\&\quad-\mu_0\varepsilon_0\sum_{\omega_1}\boldsymbol{\chi}^{(2)}(\omega_1,\omega_2)\\&\quad:\mathbf{E}_{eff}(\omega_1,\mathbf{r})\sum_{\omega_2}\mathbf{E}_{eff}(\omega_2,\mathbf{r})\\&\quad\times(\omega_1+\omega_2)^2e^{-i(\omega_1+\omega_2)t}.\end{aligned} \tag{14}$$

For each corresponding frequency component, we have

$$\nabla^2 \mathbf{E}_{eff}(\omega,\mathbf{r}) = -\mu_0\varepsilon_0\omega^2\varepsilon(\omega)\mathbf{E}_{eff}(\omega,\mathbf{r}) - \mu_0\varepsilon_0\omega^2\mathbf{P}^{(2)}_{eff}(\omega), \tag{15}$$

where

$$\mathbf{P}^{(2)}_{eff}(\omega) = \sum_{\omega_1}\sum_{\omega_2}\boldsymbol{\chi}^{(2)}(\omega_1,\omega_2):\mathbf{E}_{eff}(\omega_1,\mathbf{r})\mathbf{E}_{eff}(\omega_2,\mathbf{r})\delta_{\omega,\omega_1+\omega_2},$$

and

$$\delta_{\omega,\omega_1+\omega_2} = \begin{cases} 1, & \omega = \omega_1+\omega_2 \\ 0, & \omega \neq \omega_1+\omega_2. \end{cases}$$

For simplification, in our solution, we assume plane wave propagating along the z axis and regard the excitation of the nonlinear interaction as a perturbation, so the solution for Eq. (15) has the following form:

$$\mathbf{E}_{eff}(\omega,\mathbf{z}) = E_{eff}(\omega,z)[\mathbf{a}(\omega)+\mathbf{b}(\omega,z)]e^{ik(\omega)z},$$

where $\mathbf{b}(\omega,z)$ is the variation of the electric field vector caused by the nonlinear interactions. $E_{eff}(\omega,z)$ is a slowly varying function of propagation distance z, and $\mathbf{b}(\omega,z)$ has little changes. Associated with Eq. (13) and ignoring the terms of $\partial^2 E_{eff}/\partial z^2$, $\partial\mathbf{b}/\partial z$, and $\partial^2\mathbf{b}/\partial z^2$ by taking the slowly varying amplitude approximation, we reduce the second-order differential equation (15) to a first-order differential equation

$$\begin{aligned}\frac{d\mathbf{E}_{eff}(\omega,z)}{dz} &= \frac{i\varepsilon_0\mu_0\omega^2}{2k(\omega)}\mathbf{P}^{(2)}_{eff}(\omega,z)e^{-ik(\omega)z} \\ &= \frac{i\varepsilon_0\mu_0\omega^2}{2k(\omega)}\sum_{\omega_1}\sum_{\omega_2}\boldsymbol{\chi}^{(2)}(\omega_1,\omega_2) \\ &\quad :\mathbf{E}_{eff}(\omega_1,z)\mathbf{E}_{eff}(\omega_2,z)\delta_{\omega,\omega_1+\omega_2}e^{-ik(\omega)z}. \end{aligned}\tag{16}$$

The factor $\delta_{\omega,\omega_1+\omega_2}$ ensures the law of energy conservation. ω, ω_1, and ω_2 here are the different frequency components of relevant nonlinear interactions. Equation (16) describes the electric field evolution of any certain frequency when a pulse travels through a nonlinear crystal.

As a general case, we apply the above method to simulate the SHG process of a laser pulse. Assuming that all the light propagates along the z-axis, all the electric field components have the same polarization along the x-axis. According to Eq. (16), the vectorial nonlinear coupled wave equations can thus be written as the following series of scalar nonlinear coupled wave equations:

$$\begin{aligned}\frac{dE^{UP}_{eff,q}(\omega_q)}{dz} &= \frac{i\omega_q}{2n(\omega_q)c}d_{eff}\times\sum_{o=1}^{N}\sum_{p=1}^{N}E^{FW}_{eff,o}(\omega_o) \\ &\quad\times E^{FW}_{eff,p}(\omega_p)e^{i(k(\omega_o)+k(\omega_p)-k(\omega_q))z}\delta_{\omega_q,\omega_o+\omega_p}, \end{aligned}\tag{17}$$

$$\begin{aligned}\frac{dE^{FW}_{eff,o}(\omega_o)}{dz} &= \frac{i\omega_o}{n(\omega_o)c}d_{eff}\times\sum_{q=2}^{2N}\sum_{p=1}^{q-1}E^{UP}_{eff,q}(\omega_q) \\ &\quad\times\left[E^{FW}_{eff,p}(\omega_p)\right]^* e^{i(k(\omega_q)-k(\omega_o)-k(\omega_p))z}\delta_{\omega_q,\omega_o+\omega_p}. \end{aligned}\tag{18}$$

Here, d_{eff} is the effective second-order nonlinear coefficient and it depends on the incident angle of the fundamental light. The subscripts o and p represent the different frequency components of the fundamental light and q represents the components of the up-conversion light. k is the wave vector of each frequency component. The superscripts FW and UP refer to the fundamental light and the up-conversion light, respectively. The superscript * stands for the complex conjugate. Here, we have neglected the dispersion of the second-order nonlinear susceptibility.

The nonlinear coupled wave equations utilizing the spectral discretization of the pulse laser field are used to evaluate the nonlinear wave mixing processes of pulse laser. The spectrum of the fundamental light is discretized into N sets of monochromatic plane waves. Following the same discretization rule, $2N$–1 sets of the up-conversion light are taken into consideration. Equations (17) and (18) show that all frequency components are involved in a series of nonlinear interactions under the law of energy conservation, including a chain of SHG ($\omega_o = \omega_p$) and SFG ($\omega_o \neq \omega_p$) processes whether or not the phase matching condition is satisfied. The contributions of each nonlinear process are determined by the corresponding phase mismatching factors and amplitude of the corresponding electric field. As all of the nonlinear interactions are tightly coupled, those series of $3N$–1 nonlinear coupled equations can be solved numerically by using the third-order Runge-Kutta method simultaneously.

III. SIMULATION RESULTS

The above theoretical method is applied to evaluate SHG of ultrashort pulse laser in a β-barium borate (β-BBO) nonlinear crystal. The spectrum of the fundamental light has been measured experimentally from a Ti:sapphire regenerative amplifier as shown in Fig. 1, which spans a wavelength range from 750 to 820 nm. The output pulse energy is about 1 mJ at 1 kHz with 40 fs duration, and the corresponding spectral line width is FHWM $\sim$ 25 nm. The pulse laser beam is slightly focused on a spot 8 mm in diameter. The relevant second-order nonlinear coefficient of β-BBO is taken from Ref. 19 and the dispersion of index is taken from Ref. 20. The type-I phase matching angle is set at $\theta = 29.9°$, $\varphi = 0°$,

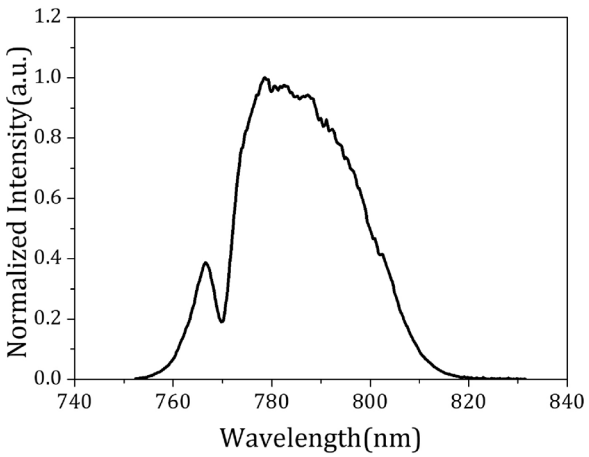

FIG. 1. The spectrum of 40 fs Ti:sapphire regenerative amplifier.

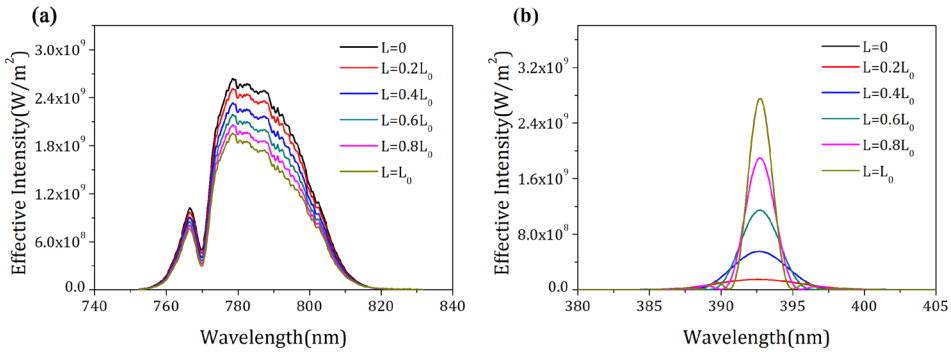

FIG. 2. Calculation result of the spectral evolution of (a) FW and (b) SHW along the transport distance L of 1 mm-thick β-BBO.

which fulfills the phase matching condition at the pump wavelength of 786 nm. The thickness of β-BBO crystal is $L_0 = 1$ mm. The spectrum of pump wave is split into $N = 351$ sets, and the angular frequency step is $\Delta\omega = 2\pi\Delta f$, where frequency step is $\Delta f = 0.109$ THz in numerical simulations. Note that the number 351 is not a special value. By using this discrete number of spectral components, the numerical result has already been convergent, and the accuracy is enough for experimental estimation. When further increasing this number of discrete spectral components, the calculation becomes more accurate but the numerical burden increases rapidly. On the other hand, decrease in the discrete number of spectral components may lead to inaccurate calculation result.

To illustrate the dynamics of energy transfer, we calculate the spectral evolution of the fundamental wave (FW) and second harmonic wave (SHW) along the transport distance L of 1 mm-thick β-BBO crystal, as plotted in Fig. 2. In the calculation, the SHW central wavelength locates at 392.7 nm as designed, the spectral FWHM bandwidth is FWHM = 1.95 nm, and the overall conversion efficiency of SHG is 28.5%. The SHG spectral FWHM bandwidth entirely stems from the second-order nonlinearities of SHG and SFG. The evolutionary behavior of FW wave indicates that the energy within the whole frequency range transfers to SHW under the combined actions of SHG and SFG processes. Because of the restriction by β-BBO dispersion, the phase matching condition changes with the wavelength of fundamental pulse, which prominently decreases the conversion efficiency. But the chains of relevant nonlinear interactions will reinforce corresponding processes.

In a practical experiment, the alignment of the fundamental wave may not be perfect. The tolerance of the incident angle must be taken into consideration. The calculated SHG conversion efficiency varying with the incident angle of FW is plotted in Fig. 3. The conversion efficiency within the range of 29.63° to 30.21° is above 20%. Numerical results reveal that the poor alignment condition leads to the decrease in conversion efficiency. The corresponding SHW spectra in different incident angles are plotted in Fig. 4. The phenomenon of spectral shifting in deviation of the incident angle is found, which is derived from the change in the condition of phase matching. The offset of peak shifting is about 10 nm/deg. The spatial distribution of the fundamental wave can lead to the spectral broadening of SHG and decrease in the conversion efficiency inevitably. In Fig. 5, we plot the calculated SHG spectrum when considering the divergent angle of 0.1° for the incident FW beam, which is more accordant with the practical experimental condition. Eventually, a 27.56% conversion efficiency with a 3.66 nm FHWM bandwidth can be evaluated in accompany with the effect of spectral broadening.

IV. COMPARISON WITH EXPERIMENTAL RESULTS AND DICUSSION

To see whether or not the BNCWT is accurate, we consider a practical experiment and compare our theoretical calculation with the experimental data. The experimental setup is schematically illustrated in Fig. 6. The above-mentioned

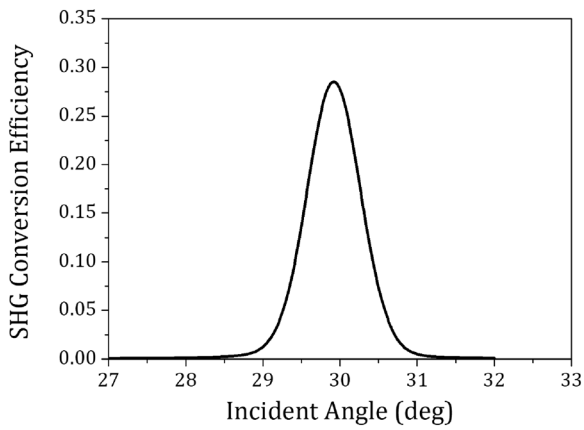

FIG. 3. SHG conversion efficiency distribution in variance with the incident angle, exhibiting a FWHM of 0.82°.

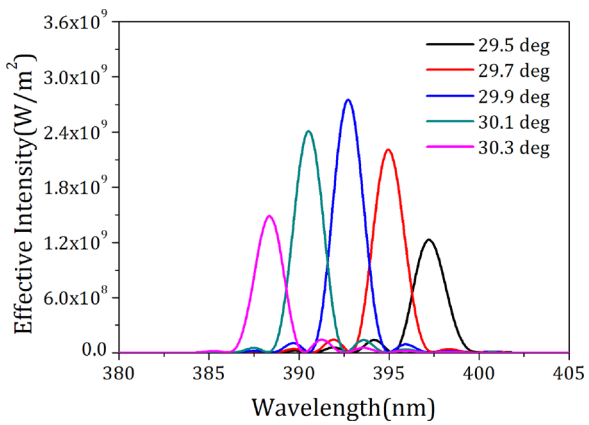

FIG. 4. Calculated distribution of SHG spectra in different incident angles.

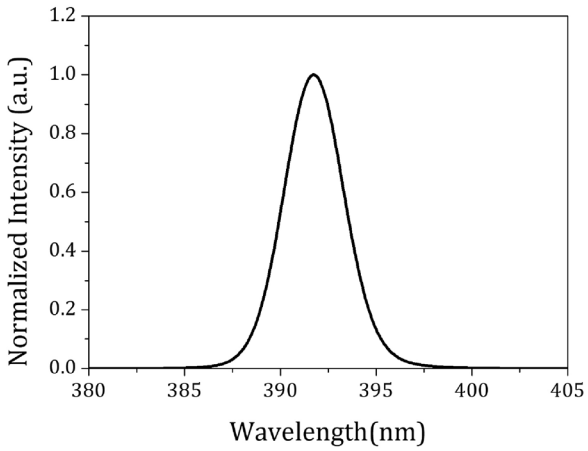

FIG. 5. Calculated SHG spectrum considering the divergent angle of 0.1° for the fundamental light beam at the phase matching angle.

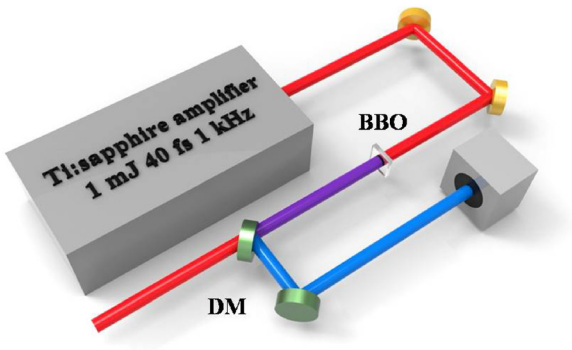

FIG. 6. Schematic illustration of the experiment layout.

Ti:sapphire regenerative amplifier acts as the fundamental laser source. The laser beam is collimated to 8 mm in diameter. A 1 mm-thick type-I phase matching β-BBO is chosen as the SHG crystal at an appropriate phase matching angle. A dichroic mirror (DM) is set to separate the pump FW beam and SHW beam. The experimental data are taken by using a UV-visible spectroscopy and power meter. The experimental SHG spectrum is plotted in Fig. 7, together with the result from the theoretical simulation. The strong SHG peak lies at nearly 392 nm. The fitting FWHM in spectrum is 3.82 nm and the SHG conversion efficiency is about 25% in the measurement data, in good agreement with the theoretical calculations. From the aspect of the conversion efficiency, the theoretical method provides a reasonable estimation. The deviation in spectrum may depend on the spectral broadening effect from the third-order nonlinearity in nonlinear media in practical experiment, which has been neglected in theory. Moreover, we measure the condition of the angle tolerance, namely, the SHG efficiency along with the deviation of the incident angle of pump laser beam away from the perfect phase matching angle. The experimental results are shown in Fig. 8 along with the calculated result. Comparison between theory and experiment in terms of several critical physical parameters shows the favorable consistency. This indicates that our BNCWT theoretical method is an efficient and valid approach to evaluate the SHG process for practical needs. The small discrepancy between theory and experiment in the shoulder of the angle dependence curve as found in Fig. 8 is probably owing to the quality of β-BBO sample.

V. CONCLUSION

In summary, we have presented a theoretical method called BNCWT to simulate SHG of an ultrashort laser pulse propagating within nonlinear optical media. In the BNCWT, the whole spectrum of the pulse laser is discretized into a series of frequency components, and each component is modeled by a monochromatic wave. The SHG problem is then described by a series of nonlinear coupled wave equations reflecting SHG and SFG for all the frequency components and their mutual complicated coupling. These multiple SHG and SFG nonlinear processes can be numerically solved by the third-order Runge-Kunta method. The BNCWT has been applied to evaluate the SHG process in a 1 mm-thick β-BBO crystal excited by a 40 fs 1 mJ Ti:sapphire regenerative amplifier, and in particular to calculate several critical physical parameters such as the bandwidth and conversion efficiency of SHG. Experiment has also been adopted and the agreement between theory and experiment is quite good in terms of these critical parameters. This agreement strongly supports the efficiency and effectiveness of the proposed BNCWT in

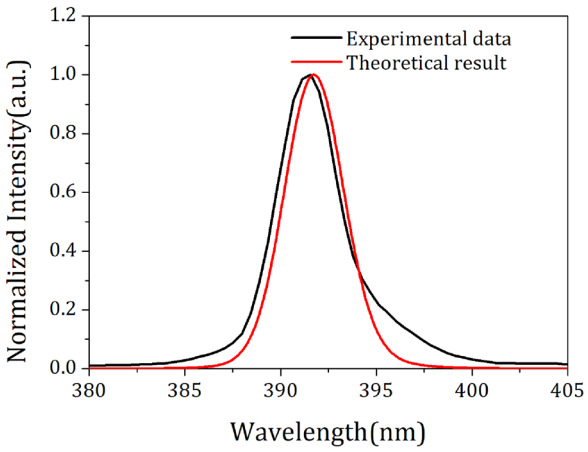

FIG. 7. Measured spectrum of SHG with fitting FWHM bandwidth of 3.82 nm pumped by 40 fs 1 mJ ultrashort pulse laser.

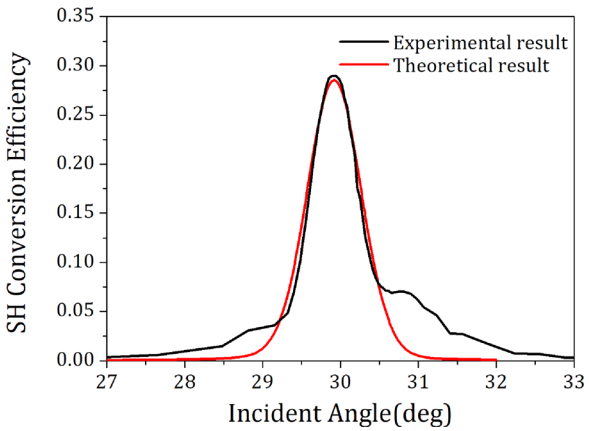

FIG. 8. The measured conversion efficiencies of SHG varying with the incident angle.

solving nonlinear optics for ultrashort pulse laser within nonlinear optical media. The study also reveals the critical importance of considering all relevant nonlinear processes in the broadband (or ultrafast) nonlinear optics. The developed numerical method can be very beneficial for estimating, explaining, and designing practical nonlinear materials to realize desirable nonlinear optical functionalities, with SHG for ultrashort pulse laser being a prominent example.

ACKNOWLEDGMENTS

This work was supported by the National Natural Science Foundation of China, Grant Nos. 11434017 and 11604101, China Postdoctoral Science Foundation Grant No. 2016M600651, and Guangdong Innovative and Entrepreneurial Research Team Program, Grant No. 2016ZT06C594.

[1]J. Armstrong, N. Bloembergen, J. Ducuing, and P. Pershan, Phys. Rev. **127**, 1918 (1962).
[2]G. Sansone, E. Benedetti, F. Calegari, C. Vozzi, L. Avaldi, R. Flammini, L. Poletto, P. Villoresi, C. Altucci, R. Velotta, S. Stagira, S. De Silvestri, and M. Nisoli, "Isolated single-cycle attosecond pulses," Science **314**, 443–446 (2006).
[3]H. S. Chan, Z. M. Hsieh, W. H. Liang, A. H. Kung, C. K. Lee, C. J. Lai, R. P. Pan, and L. H. Peng, "Synthesis and measurement of ultrafast waveforms from five discrete optical harmonic," Science **331**, 1165–1168 (2011).
[4]P. M. Paul, E. S. Toma, P. Breger, G. Mullot, F. Auge, P. Balcou, H. G. Muller, and P. Agostini, "Observation of a train of attosecond pulses from high harmonic generation," Science **292**, 1689–1692 (2001).
[5]M. Hentschel, R. Kienberger, C. Spielmann, G. A. Reider, N. Milosevic, T. Brabec, P. Corkum, U. Heinzmann, M. Drescher, and F. Krausz, "Attosecond metrology," Nature **414**, 509–513 (2001).
[6]T. A. Birks, W. J. Wadsworth, and P. St. J. Russell, "Supercontinuum generation in tapered fibers," Opt. Lett. **25**, 1415–1417 (2000).
[7]B. Q. Chen, C. Zhang, C. Y. Hu, R. J. Liu, and Z. Y. Li, "High-efficiency broadband high-harmonic generation from a single quasi-phase-matching nonlinear crystal," Phys. Rev. Lett. **115**, 083902 (2015).
[8]M. A. Dreger and J. K. Mclver, "Second-harmonic generation in a nonlinear, anisotropic medium with diffraction and depletion," J. Opt. Soc. Am. B **7**, 776–784 (1990).
[9]P. Pliszka and P. P. Banerjee, "Nonlinear transverse effects in second-harmonic generation," J. Opt. Soc. Am. B **10**, 1810–1819 (1993).
[10]A. V. Smith and M. S. Bowers, "Phase distortions in sum and difference-frequency mixing in crystals," J. Opt. Soc. Am. B **12**, 49–57 (1995).
[11]A. V. Smith, W. J. Alford, T. D. Raymond, and M. S. Bowers, "Comparison of a numerical model with measured performance of a seeded, nanosecond KTP optical parametric oscillator," J. Opt. Soc. Am. B **12**, 2253–2260 (1995).
[12]G. Arisholm, "General numerical methods for simulating second-order nonlinear interactions in birefringent media," J. Opt. Soc. Am. B **14**, 2543–2549 (1997).
[13]I. Gusachenko and M. Schanne-Klein, "Numerical simulation of polarization-resolved second-harmonic microscopy in birefringent media," Phys. Rev. A **88**, 053811 (2013).
[14]J. D. McMullen, "Optical parametric interactions in isotropic materials using a phase-corrected stack of nonlinear dielectric plates," J. Appl. Phys. **46**, 3076–3081 (1975).
[15]M. M. Fejer, G. A. Magel, D. H. Jundt, and R. L. Byer, "Quasi-phase-matched second harmonic generation: Tuning and tolerances," IEEE J. Quantum Electron. **28**, 2631–2654 (1992).
[16]M. L. Ren and Z. Y. Li, "Exact iterative solution of second harmonic generation in quasi-phase-matched structures," Opt. Express **18**, 7289–7299 (2010).
[17]M. L. Ren and Z. Y. Li, "An effective susceptibility model for exact solution of second harmonic generation in general quasi–phase-matched structures," Eur. Phys. Lett. **94**, 44003 (2011).
[18]C. Y. Hu and Z. Y. Li, "An effective nonlinear susceptibility model for general three-wave mixing in quasi-phase-matching structure," J. Appl. Phys. **121**, 123110 (2017).
[19]R. S. Klein, G. E. Kugel, A. Maillard, A. Sifi, and K. Polgár, "Absolute non-linear optical coefficients measurements of BBO single crystal and determination of angular acceptance by second harmonic generation," Opt. Mater. **22**, 163–169 (2003).
[20]G. C. Bhar, S. Das, and U. Chatterjee, "Evaluation of beta barium borate crystal for nonlinear devices," Appl. Opt. **15**, 202–204 (1989).